Imaging in pleural mesothelioma: A review of the 14th International Conference of the International Mesothelioma Interest Group

Samuel G. Armato III[a,*], Roslyn J. Francis[b,c], Sharyn I. Katz[d], Guntulu Ak[e], Isabelle Opitz[f], Eyjolfur Gudmundsson[a], Kevin G. Blyth[g,h], Ashish Gupta[i]

[a] Department of Radiology, The University of Chicago, Chicago, Illinois, USA
[b] Department of Nuclear Medicine, Sir Charles Gairdner Hospital, Perth, Western Australia, Australia
[c] Faculty of Health and Medical Sciences, University of Western Australia Medical School, Australia
[d] Department of Radiology, University of Pennsylvania Perelman School of Medicine, Philadelphia, Pennsylvania, USA
[e] Lung and Pleural Cancers Research and Clinical Center, Eskisehir Osmangazi University, Eskisehir, Turkey
[f] Division of Thoracic Surgery, University Hospital Zurich, Zurich, Switzerland
[g] Glasgow Pleural Disease Unit, Queen Elizabeth University Hospital, Glasgow, UK
[h] Institute of Infection, Immunity & Inflammation, University of Glasgow, UK
[i] Department of Radiology, The Ottawa Hospital, Ottawa, Ontario, Canada

ARTICLE INFO

ABSTRACT

Mesothelioma patients rely on the information their clinical team obtains from medical imaging. Whether x-ray-based computed tomography (CT) or magnetic resonance imaging (MRI) based on local magnetic fields within a patient's tissues, different modalities generate images with uniquely different appearances and information content due to the physical differences of the image-acquisition process. Researchers are developing sophisticated ways to extract a greater amount of the information contained within these images. This paper summarizes the imaging-based research presented orally at the 2018 International Conference of the International Mesothelioma Interest Group (iMig) in Ottawa, Ontario, Canada, held May 2–5, 2018. Presented topics included advances in the imaging of preclinical mesothelioma models to inform clinical therapeutic strategies, optimization of the time delay between contrast administration and image acquisition for maximized enhancement of mesothelioma tumor on CT, an investigation of image-based criteria for clinical tumor and nodal staging of mesothelioma by contrast-enhanced CT, an investigation of methods for the extraction of mesothelioma tumor volume from MRI and the association of volume with patient survival, the use of deep learning for mesothelioma tumor segmentation in CT, and an evaluation of CT-based radiomics for the prognosis of mesothelioma patient survival.

1. Introduction

The biennial conference of the International Mesothelioma Interest Group (iMig) includes a dedicated imaging session that features recent advances in imaging research and clinical adaptation of imaging technology in the diagnosis and evaluation of mesothelioma [1–5]. Imaging continues to play a critical role in the evaluation and surveillance of malignant pleural mesothelioma (MPM) patients, and researchers continue to seek ways to enhance, optimize, and extend the many roles that imaging has in the MPM setting. Imaging research has two broad categories: (1) research to improve or optimize image acquisition and (2) research to enhance image visualization post acquisition or to extract quantitative data for task-specific image analysis. This paper summarizes research from both categories presented in the imaging session of the 2018 International Conference of the International Mesothelioma Interest Group in Ottawa, Ontario, Canada, in May 2018.

In the era of precision medicine, imaging agents, imaging technology, and imaging applications are rapidly expanding. Positron emission tomography (PET)-based molecular imaging in the preclinical setting is emerging as a powerful tool to accelerate development of therapies by allowing researchers to visualize (and hence better understand) the mechanisms of action in vivo, which, in turn, leads to more intelligent drug development [6].

Image quality and the diagnostic utility of images depend on proper selection of image acquisition parameters, which include the time delay between injection of contrast medium and initiation of imaging for

---

computed tomography (CT) and magnetic resonance imaging (MRI). Standard contrast time delays have evolved for clinical imaging of the chest; however, the location of MPM tumor surrounding the outside of the lung peripherally would suggest the need for a time delay specific to MPM imaging. Such a customized imaging time delay would better maximize the visual contrast difference between MPM tumor and the surrounding tissues that, for CT, have similar endogenous x-ray attenuation properties. Subsequent computerized image analysis methods would also benefit from the resulting enhanced contrast difference. Until recently [5,7], however, optimization of the contrast time delay for MR and CT has been ignored in the literature.

The CT-based assessment of MPM clinical stage has been the subject of recent scrutiny [8–12]. A validated metric for assigning to MPM patients a stage that reflects patient prognosis and correlates with patient outcome is essential for proper consideration of treatment options. The unique morphology, anatomic location, and growth patterns of MPM require an approach to staging that differs from the traditional rubric of stage, specifically with regard to T ("tumor") and N ("node") stage. Novel ways of combining visually assessed imaging information into the staging system are being investigated with the goal of improved correlation between assigned stage and patient survival.

Information visually obtained from CT scans (or images from any medical imaging modality) is inherently subjective. Intrinsic, quantitative information may be extracted from medical images by using the numeric values (the "pixel values") that are stored in each image file and subsequently displayed as differing levels of brightness for the benefit of human observers. The mathematical manipulation of these values forms the basis of image processing (for enhanced visualization), computer vision (for automated detection and characterization of disease), and radiomics (for the extraction of quantitative measures of structure morphology and texture) [13]. A more recent term to describe a concept that has been in the literature for decades, "radiomics" has emerged as a powerful tool across a wide range of radiologic tasks, from the classification of lung nodules as benign or malignant [14] to the prediction of tumor recurrence [15]. The extraction of radiomics features from MPM tumor to identify a subset of such features that best correlate with patient survival should prove equally valuable.

Prior to the computerized analysis of MPM tumor in medical images, knowledge of which pixels belong to the tumor is required. In other words, the tumor must be "segmented" from the rest of the anatomy captured in the image, and the complete tumor volume must be identified. Segmentation of anatomic and pathologic structures from within medical images is a challenging task [16]. Advanced methods to segment MPM tumor in CT and MRI through deep learning and more traditional thresholding-based approaches will benefit both tumor volume calculations as well as radiomics-based assessment of tumor characteristics.

2. Preclinical imaging

Preclinical research is important for the understanding of tumor biology and for the development of new therapies to control and treat disease. In mesothelioma, preclinical models are used to test the therapeutic effect and biodistribution of new treatments in an in vivo setting, prior to clinical trials. Mesothelioma models may also be used to explore tumor growth patterns, investigate the tumor microenvironment, and improve understanding of tumor spread. Imaging has the potential to add value to small animal research by noninvasively obtaining information on cell processes, tumor microenvironment, tumor growth, and tumor response to treatment. Imaging can be performed serially (with each animal serving as its own control) to better understand treatment effect and minimize the number of animals required [17].

Animal models include xenograft tumors (human cell lines implanted in immunosuppressed mice) implanted as subcutaneous flank tumors or orthotopically at the site of the primary tumor source [18]; in mesothelioma, orthotopic models may include pleural or peritoneal

implantation. Alternatively, genetically modified mice may be bred to develop de novo tumors that parallel the development of human cancers [18]. The MexTAg mouse model is an inducible tumor model [19,20]: on exposure to asbestos, the genetically modified mice develop mesothelioma with a latency of 20–40 weeks [20]. This model provides an important platform for addressing a number of questions regarding mesothelioma tumor development and can be used to test prevention and early intervention strategies [20]. While subcutaneous models may be monitored by visual assessment and caliper measurements, growth or treatment response in orthotopic and de novo tumors cannot be readily observed externally, as these tumors develop on the pleura or peritoneum. Consequently, imaging is needed to non-invasively monitor these tumors to evaluate growth pattern and therapeutic efficacy.

In preclinical imaging, CT has relatively poor soft tissue resolution, and MRI is frequently performed to confirm anatomic detail. Co-registration of PET and MRI provides both functional and anatomic imaging data, which then can be quantified for objective, computational analysis. 18F-fluorodeoxyglucose (FDG) PET using a small animal PET camera is the most ideal imaging modality for monitoring tumor growth and therapy response in the preclinical setting. In the MexTAg de novo tumor model, FDG-PET imaging may facilitate the detection of peritoneal tumors and allow therapeutic intervention and monitoring (Fig. 1). The development of genetic mouse models is expensive, and imaging has an important emerging role in optimizing experiments with regard to timing of interventions and monitoring of outcomes.

Other PET tracers may be used to assess mesothelioma mouse models. One such example is 18F-fluoromisonidazole (FMISO) for the evaluation of hypoxia. In clinical trials, hypoxia present in human mesothelioma tumors may contribute to resistance to therapy [21]. Modulation of hypoxia may increase therapeutic efficacy; therefore, the monitoring of hypoxia in preclinical models may lead to the development of strategies that can be translated to human clinical trials [4].

In summary, preclinical imaging, specifically with PET, may have several roles. These roles include characterizing preclinical models and establishing how closely preclinical models parallel tumors in the clinical setting, monitoring the rate and characteristics of tumor growth (in particular for de novo tumor models), assessing efficacy of new therapies over time with serial time-point imaging, and developing imaging endpoints that correlate with efficacy of treatment and can translate into "intelligent" clinical trial design. Multiple imaging modalities and imaging probes are available to be matched with the experimental question under investigation.
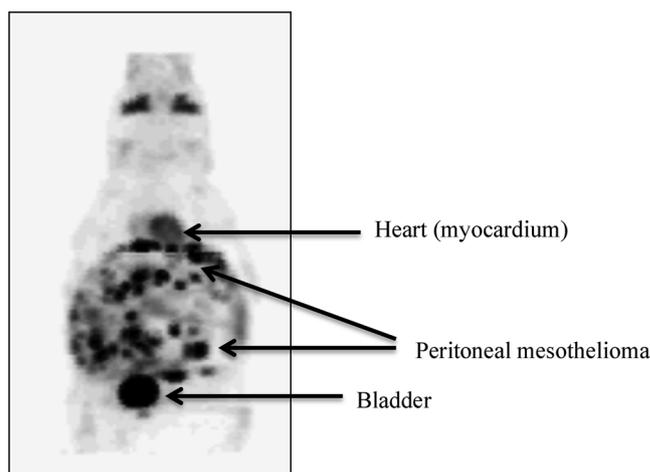

Fig. 1. FDG-PET maximum intensity projection image of a MexTAg genetically modified mouse. The multiple small foci of FDG activity in the abdomen represent peritoneal mesothelioma (Image courtesy of C. Robinson; acknowledgment to ACRF Cancer Imaging Facility, Perth, Australia)

3. Dynamic enhancement with CT

While most modern CT scanners have high spatial resolution capable of resolving structures to under 1 mm in size, accurate staging of MPM remains a diagnostic challenge on CT. For example, in a study by Rusch et al. [22] as many as 80% of MPM patients with stage 1 and 2 disease and 23% of patients with stage 3 disease were upstaged postoperatively. This inaccuracy in pre-operative staging ("clinical staging") with CT is partly due to similarities between the tissue attenuation of tumor and adjacent structures including chest wall, complex pleural fluid, and atelectatic lung [23]. To improve tissue contrast (i.e., to enhance the differential attenuation of tumor with respect to adjacent structures), an intravenous (IV) contrast medium can be administered; the timing of image acquisition with respect to the administration of this contrast medium will impact the conspicuity of imaged structures. The standard time delay between contrast administration and CT image acquisition is typically 40–60 s for clinically optimal enhancement of tissues and opacification of arterial and venous structures. Katz and colleagues have demonstrated that the optimal timing for enhancement of MPM on MRI is between 150 and 300 s following the administration of MRI-specific contrast medium [5,7]; in the present study, this group examined whether the optimal timing for enhancement of MPM on CT occurs at a time point later than the clinical standard.

Ten adult MPM patients planned for pleurectomy were enrolled in a prospective, exploratory imaging clinical trial approved by the local institutional review board. Patients with maximum pleural tumor thickness less than 1 cm, prior pleurectomy, or prior pleural radiation were excluded. All patients underwent contrast-enhanced CT of pleural tumor at 0 s, 20 s, 40 s, 60 s, 2 min, 4 min, 6 min, 8 min, and 10 min following administration of IV contrast medium to create a dynamic series, and tumor tissue attenuation was measured at each phase. Using best-fit model curves, predicted maximum attenuation values and the time delays at which they occur were estimated using non-linear regression.

Tumor enhancement kinetics of all 10 patients was displayed as maximal tumor tissue attenuation as a function of time. Best-fit statistical analysis (Fig. 2) revealed an estimated optimal time delay in the range of 230–300 s following IV contrast administration. This small prospective clinical trial found that maximal MPM CT contrast enhancement occurs at a time delay greater than the conventional time delay for CT chest imaging (usually 40–60 s). Further study of the impact of delayed phase enhancement on radiologic MPM staging accuracy and therapy response assessment is warranted, ideally in a multicenter prospective clinical trial.

By optimizing mesothelioma tumor enhancement, and hence tissue contrast, improved staging accuracy with CT might be achieved.
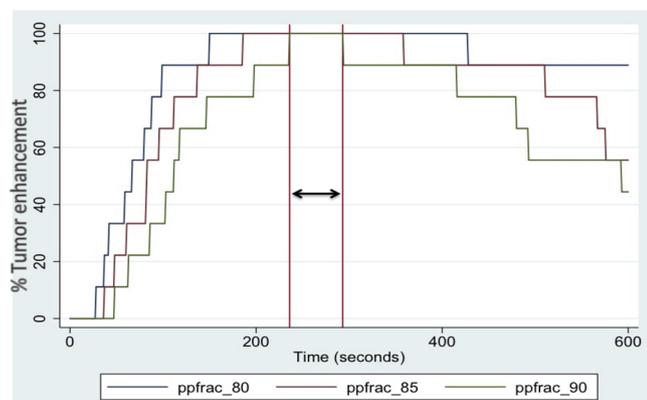
Moreover, improved tissue contrast between tumor and adjacent structures with similar attenuation (e.g., chest wall and complex pleural fluid) may translate into better performance of semi-automated and automated segmentation tools that are in use and under development. In addition to optimizing the timing of image acquisition following IV contrast, it would also be of interest to explore other technical parameters that may impact enhancement on CT including rate of IV contrast delivery and contrast dose. By systematically fine-tuning these CT imaging parameters, the best possible quality of mesothelioma imaging on CT may be achieved, which has implications both for clinical management of patients and for research and development of imaging software tools.

4. Descriptors for clinical staging

Stage is one of the most important prognostic factors in MPM and has gained international attention [8–12]. The staging of MPM is unique due to its non-spherical growth patterns along the pleural surface, the assessment of T stage based on local invasion rather than tumor size, and lymphatic drainage involving unusual locations such as internal mammary, cardiophrenic, and intercostal regions. Contrast-enhanced CT remains the most-frequent initial imaging technique for MPM clinical staging [24–26]. In recommendations for the Eighth Edition of the TNM Classification for Pleural Mesothelioma Staging, clinical T3 and T4 survival curves overlap, the N2 category is merged with the N1 category, the N3 category is merged with the N2 category, and measurement of pleural thickness is advocated for its prognostic value [9,10]. It is therefore important to improve clinical staging for both disease prognosis and treatment choice selection in MPM. Ak and colleagues analyzed novel imaging criteria for clinical T and N staging of MPM by contrast-enhanced CT.

The pretreatment CT scans of 210 MPM patients who were diagnosed and treated between 2010–2016 were retrospectively and blindly reviewed. Patients with distant metastasis (n = 14) were excluded. The new staging criteria were tested for their association with patient survival (calculated from date of diagnosis); these criteria included tumor morphologic appearance (homogenous rind, heterogeneous rind, heterogeneous diffuse disease, localized tumor, or pleural fluid only), maximum thickness of the tumor, anatomic location of this maximum thickness, predominant intrathoracic region of the tumor, invasion of major anatomic structures, and pattern of lymph node metastasis (no metastasis, metastasis to lymph nodes within the lung cancer lymph node map, metastasis to lymph nodes outside the lung cancer map, or metastasis to lymph nodes both within and outside the map). Kaplan-Meier survival, log-rank, receiver operating characteristic (ROC), and univariate analyses were performed.

Average age was 62 ± 11.6 years; 120 (61%) patients were male. Epithelioid, biphasic, and sarcomatoid histology was shown in 140 (71%), 36 (18%), and 17 (9%) patients, respectively (histological subtype could not be identified in three patients). Patients underwent best supportive care (n = 26), chemotherapy (n = 107), or multimodality treatment including surgery (n = 63). Mean follow-up was 19.5 ± 15.8 months. Median survival was 14.2 months (95% CI: 10.6–17.8 months), with a 2-year survival of 31%. The median survival times for patients with epithelioid, biphasic, and sarcomatoid histologies were 20.1, 10.5, and 7 months, respectively (significantly different, $p < 0.001$).

There was a separation of curves according to morphologic appearance of the tumor. Median survival times for patients with (1) fluid only and localized tumor combined, (2) heterogeneous diffuse disease, and (3) heterogeneous/homogenous rinds were 20.9, 14.6, and 11.2 months, respectively. Patients with homogenous and heterogeneous rinds had the worst survival (p = 0.031; 95% CI: 8.9–13.3 months) (Fig. 3a). The average maximum tumor thickness was 21.7 ± 19.8 mm. The presence of any pleural thickening, regardless of measured thickness, was associated with poor survival. Location of the thickest part of tumor was not associated with survival. Metastasis to lymph nodes both within and

Fig. 2. Best-fit analysis of time-enhancement curves for MPM. At a time delay range of 230–300 s (double arrow), > 95% of maximal tumor enhancement is achieved for all 10 patients.
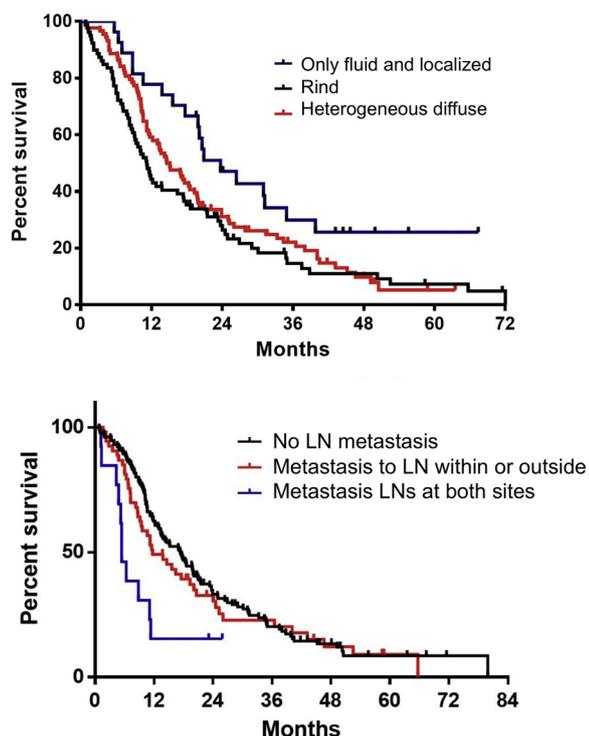
Fig. 3. Top: Kaplan-Meier survival curves for types of pleural thickening. Bottom: Kaplan-Meier survival curves for lymph node metastasis.

outside the lung cancer lymph node map was associated with worse survival: median survival times for patients with metastasis within, outside, and both within and outside the lung cancer lymph node map were 17.3, 11.7, and 5.4 months, respectively (p = 0.003; 95% CI: 5–5.8 months) (Fig. 3b).

Rind-type pleural thickening and concurrent lymph node metastasis to nodes both within and outside the lung cancer lymph node map were associated with poorer survival and should be considered in future MPM staging efforts. Tumor thickness should be evaluated in a larger series to determine whether a threshold exists that better correlates with survival. Given the strong dependence of survival on tumor histology, staging should perhaps be evaluated separately for epithelioid and other histologic subtypes.

5. Radiomics for outcomes prediction

Tumor volumetry has been identified as an important prognostic factor for overall survival (OS) of MPM patients. Radiomics is a mathematical approach to describing and quantifying the shape, intensity, and texture of a tumor on radiologic imaging in a more sophisticated

and comprehensive way as compared with volumetry alone. Radiomics has proven to be prognostic for local tumor control in head and neck cancer and for OS after definitive radiotherapy in lung cancer [27,28]. Opitz and colleagues evaluated radiomic features in CT images as a prognostic factor for OS in MPM patients.

The primary tumor was delineated in 30 patients with proven MPM in CT images performed at the time of primary diagnosis. 1404 radiomic features of shape (n = 18), intensity (n = 17), texture (relation of an individual pixel to its neighborhood, n = 137), and wavelet decomposition (n = 1232) were calculated with an in-house developed software implementation (Z-Rad). Features were pre-selected based on an inter-observer robustness study (tumors contoured independently by three observers), and stable features were grouped based on average hierarchical clustering. The most prognostic feature from among each identified group of correlated features was selected and included in multivariable Cox regression for prediction of OS and progression free survival (PFS) calculated from date of diagnosis.

Median follow-up time was 14.1 months, and median OS was 14.2 months. 505 out of the 1404 radiomic features were stable, and hierarchical clustering revealed six groups of correlated and stable features. Overall, 18 features distributed over five groups of correlated features were prognostic in univariate Cox regression (the Bonferroni correction for multiple comparisons was applied), and two wavelet features were prognostic for OS in multivariable Cox regression (concordance index: 0.74, p = 0.002). Both features separated the patients into two groups with a significantly different OS (p = 0.0006) and a significantly different PFS (p = 0.003) (Fig. 4). For comparison, tumor volume was prognostic in univariate Cox regression (p = 0.01) but had a smaller concordance index (0.62).

A prognostic model for OS in MPM patients was developed based on CT image characteristics. Radiomic biomarkers had a stronger prognostic value compared with tumor volume alone. Further studies are ongoing to validate these results in a larger cohort of patients.

6. Deep learning tumor segmentation

Volumetric segmentation of MPM tumor has been a topic of interest for prognostic evaluation, tumor response assessment, and tumor staging [12,29–31]. The automated segmentation of MPM tumor, however, is challenging due to the irregular morphology of the disease, low contrast of tumor and surrounding soft-tissue structures, and variability in tumor extent and presentation. Gudmundsson and colleagues investigated the use of deep convolutional neural networks (CNNs) ("deep learning") for the segmentation of MPM tumor on CT scans [40].

The U-Net deep CNN architecture presented by Ronneberger et al. [32] was used to segment MPM tumor. As a reference standard for CNN training, visible pleural thickening was semi-automatically contoured on the axial sections of 146 chest CT scans from 87 MPM patients. Deep CNNs were trained separately for the left and right hemithorax on the two-class problem of differentiating between pleural thickening and
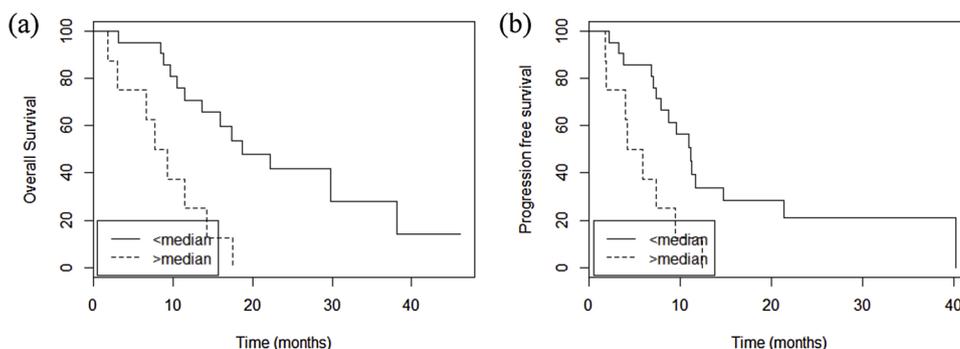

Fig. 4. (a) Overall survival curves and (b) progression-free survival curves for patients separated based on the features with the largest concordance index in univariate Cox regression.

normal thoracic tissue. A total of 4259 and 6192 axial CT sections containing segmented tumor were used to train the left- and right-hemithorax CNNs, respectively.

The average binary cross-entropy and Dice similarity coefficient (DSC) between deep CNN-predicted and reference tumor segmentations were used as measures of segmentation performance during training. DSC is an overlap metric that lies between 0 (indicating no overlap between the segmentations being compared) and 1 (indicating complete overlap). Distinct validation sets of eight patients were randomly selected to evaluate overfitting of the CNNs to the training set in each hemithorax; the networks were applied to the validation sets after each iteration over the training sets. After 50 iterations over the training sets, the deep CNNs to be applied to the test set were selected as the ones that minimized the average binary cross-entropy and maximized the average DSC on the validation set of each hemithorax.

The trained CNNs were tested on 63 axial CT sections from 17 MPM patients not included in the training or validation sets, with reference tumor segmentations on all sections provided by three radiologists. These images were part of a previously published MPM tumor segmentation method and allowed for a direct comparison with that method (hereafter referred to as the "2011 Method") [33]. The two-sided Wilcoxon signed-rank test was used to test the null hypothesis that the DSC distributions for the present deep CNN-based method and the 2011 Method were identical over the test set when compared with observer reference segmentations ($\alpha = 0.05$).

The median DSC (range) when comparing deep CNN-predicted tumor segmentations with observer reference segmentations on the test set were 0.776 (0.314-0.938), 0.688 (0.251-0.931), and 0.800 (0.308-0.952) for Observers A, B, and C, respectively. The median DSC (range) when comparing tumor segmentations obtained from the 2011 Method with observer reference segmentations on the same test set were 0.718 (0-0.938), 0.604 (0-0.902), and 0.709 (0-0.926) for Observers A, B, and C, respectively. The greater overlap with observer reference segmentations for the deep CNN-based method was significant for all observers ($p < 0.001$). Fig. 5 presents, for the reference segmentation of each observer for each case in the test set, the DSC value of the present deep CNN-based method plotted against the corresponding DSC value of the 2011 Method.
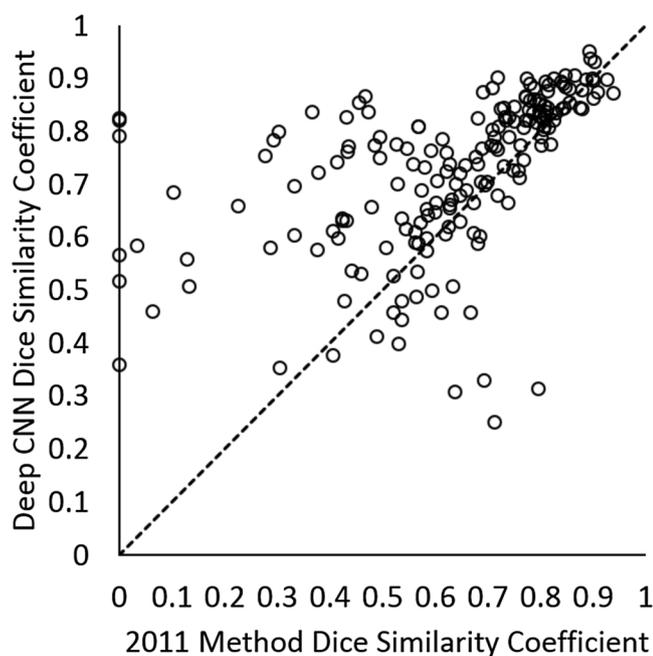

Fig. 5. DSC values for the deep CNN-based method and the 2011 Method when compared with observer reference segmentations (across all observers) on the test set of 63 axial CT sections. The line of equality is shown.

A deep CNN was successfully implemented for the automated segmentation of MPM tumor on CT scans. The output of the deep CNN-based method showed significantly higher overlap with three sets of observer reference segmentations when compared with a previously published MPM segmentation method. Future work will focus on improving the accuracy and robustness of this method by training on a larger set of annotated CT scans and extending the network through the use of three-dimensional convolutional filters.

7. Tumor volume from MRI

MPM exhibits an unusual, rind-like growth pattern, and primary tumor (T-) staging is currently based on the extent of pleural surface involvement and extra-pleural invasion, which makes staging more difficult than in other tumors such as lung cancer, where unidimensional tumor measurements are utilized [9,34]. Previous attempts to address this problem using volumetric analyses (generally on CT) have been limited by time-consuming and complex methods [12,31,35,36]. MRI offers higher contrast resolution than CT and is therefore potentially better suited to volumetric analyses [37,38]. In this study, Blyth and colleagues sought to determine an optimal MRI volumetric method for correlation with biomarkers drawn in the recently completed DIAPHRAGM study (ISRCTN10079972) [39], in which 639 patients with suspected pleural malignancy were recruited across 23 centers in the United Kingdom between December 2013 and December 2016. Patients recruited in Glasgow centers for whom a pleural biopsy (thoracoscopic or image-guided) was clinically indicated were eligible for the MRI sub-study; standard MRI exclusion criteria applied.

A total of 31 patients with MPM underwent gadobutrol-enhanced 3-Tesla MRI prior to pleural biopsy or any significant pleural intervention. Patients were scanned isotropically in the coronal plane during a short breath hold. Volumetric analyses were performed using Myrian® software (Intrasense, France). Manual delineation of visible parietal pleura was performed on selected slices from the 4.5-minute post-contrast scan, and shape-based interpolation was used to propagate these delineations throughout the image series to create the "contour mask." Tumor volume then was measured within this mask by region-growing-based segmentation using four different thresholding methods based on signal intensity (SI) limits derived from earlier perfusion MRI studies. Each method was evaluated in terms of analysis time, intra-observer variability, visual assessment of accurate tumor coverage, and measured error relative to a phantom containing a known volume of fluid.

Mean patient age was 76 ± 7 years; 28 patients (90%) were male. MPM histologic subtypes were epithelioid (68%, n = 21), biphasic (13%, n = 4), sarcomatoid (16%, n = 5), and mesothelioma not otherwise specified (NOS) (3%, n = 1). The optimal segmentation method was based on a contour mask SI +/- 99 (arbitrary units) (Fig. 6). Using this method, mean analysis time was 16 min, intra- and inter-observer intra-class correlation coefficients (ICC) were 0.799 (95% CI: 0.528 – 0.922) and 0.931 (95% CI: 0.816 – 0.975), respectively, and error relative to the phantom was -3.6%. Patients with higher tumor volumes (≥ 300 ml) had significantly poorer median OS (Fig. 6). The observed difference in median OS with tumor volume increased when analysis was confined to patients with epithelioid histology (21/31) and further increased when epithelioid cases with nodal or metastatic disease were excluded (18/31) (Fig. 6). Across all 31 cases, increasing tumor volume, by tertile, was associated with decreasing median OS (≤ 250 ml, 250–400 ml, ≥ 400 ml; log-rank for trend p = 0.023). Tumor volume was independently associated with OS in a multivariable Cox proportional hazards model (HR: 2.114 (1.046–4.270), p = 0.037).

In this pilot study, a novel MRI perfusion-tuned method for volumetric tumor segmentation in MPM appeared accurate and reproducible. High tumor volume was associated with reduced survival. Further studies, including validation against resected tumor volumes after extended pleurectomy/decortication, are planned.
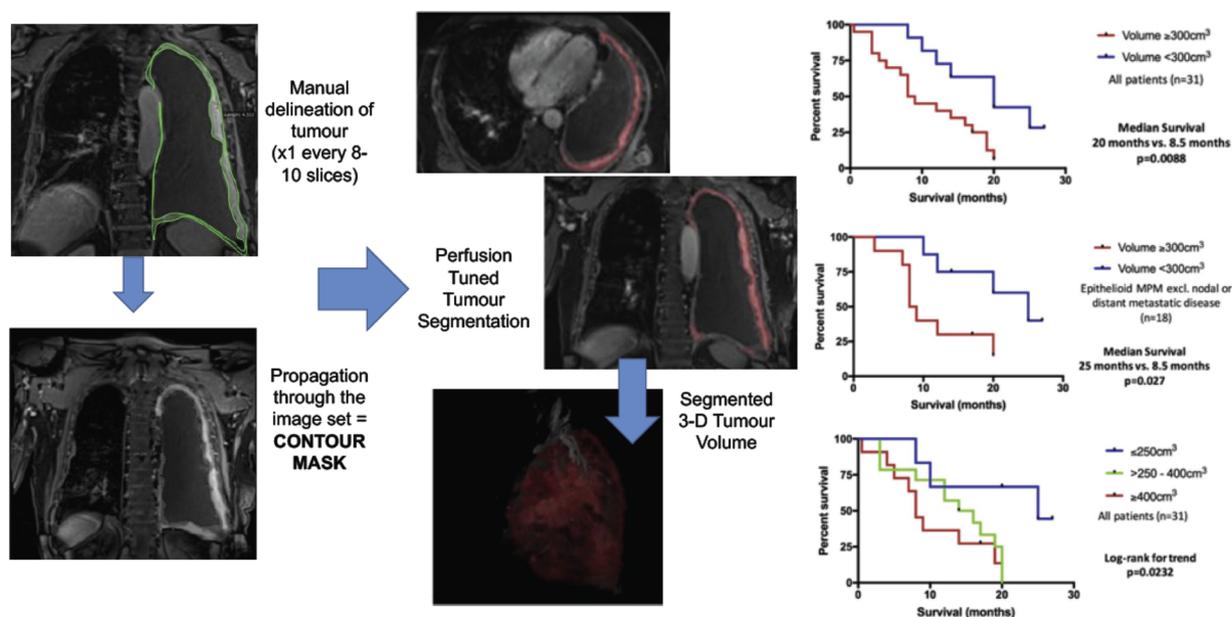
Fig. 6. Semi-automated, perfusion-tuned mesothelioma tumor segmentation at 3 T contrast-enhanced MRI. A "contour mask" is generated throughout the image series (left panels). Tumor regions are grown within this mask volume (in red, middle panels) based on pre-defined signal intensity limits. Patient survival is shown dichotomized by MRI tumor volume at 300 cm^3 and by tertile (right panels). (For interpretation of the references to colour in this figure legend, the reader is referred to the web version of this article.).

8. Conclusion

The biennial international conference of iMig provides a forum for imaging scientists with interest in mesothelioma to share their research. The topics presented at the 2018 iMig meeting are the focus of continued research effort and clinical investigation. The role of preclinical imaging using PET and MRI to provide quantifiable functional and anatomic data is expanding and serves as a valuable tool to improve understanding of tumor growth, efficacy of new therapies, and clinical trial design. Research in CT to improve the differentiation of tumor from surrounding anatomic structures by optimizing contrast delay along with an exploration of CT-based tumor morphology and nodal distribution as potential new descriptors of clinical staging were presented. Image analysis through advanced computational techniques using radiomics as a potential biomarker for prognosis and using deep convolutional neural networks for automated segmentation of tumor has opened a promising new frontier for mesothelioma research in CT. The correlation of tumor volume with survival and techniques to improve the accuracy of volume measurements using CT or MR remain topics of interest for investigators. Further advances in these and other promising aspects of imaging are expected to be presented at iMig 2020 in Brisbane, Queensland, Australia.

References

[1] S.G. Armato III, J. Entwisle, M.T. Truong, A.K. Nowak, G.L. Ceresoli, B. Zhao, R. Misri, H.L. Kindler, Current state and future directions of pleural mesothelioma imaging, Lung Cancer 59 (2008) 411–420.

[2] A.K. Nowak, S.G. Armato III, H. Yildirim, G.L. Ceresoli, R.J. Francis, Imaging in pleural mesothelioma: a review of imaging research presented at the 9th International meeting of the International Mesothelioma Interest Group, Lung Cancer 70 (2010) 1–6.

[3] S.G. Armato III, Z.E. Labby, J. Coolen, A. Klabatsa, M. Feigen, T. Persigehl, R.R. Gill, Imaging in pleural mesothelioma: a review of the 11th International Conference of the International Mesothelioma Interest Group, Lung Cancer 82 (2013) 190–196.

[4] S.G. Armato III, J. Coolen, A.K. Nowak, C. Robinson, R.R. Gill, C. Straus, A. Khanwalkar, Imaging in pleural mesothelioma: a review of the 12th International Conference of the International Mesothelioma Interest Group, Lung Cancer 90

(2015) 148–154.

[5] S.G. Armato III, K.G. Blyth, J.J. Keating, S. Katz, S. Tsim, J. Coolen, E. Gudmundsson, I. Opitz, A.K. Nowak, Imaging in pleural mesothelioma: a review of the 13th International Conference of the International Mesothelioma Interest Group, Lung Cancer 101 (2016) 48–58.

[6] I. Colombo, M. Overchuk, J. Chen, R.M. Reilly, G. Zheng, S. Lheureux, Molecular imaging in drug development: update and challenges for radiolabeled antibodies and nanotechnology, Methods 30 (2017) 23–35.

[7] A.M. Patel, I. Berger, E.P. Wileyto, U. Khalid, D.A. Torigian, A.C. Nachiappan, et al., The value of delayed phase enhanced imaging in malignant pleural mesothelioma, J. Thorac. Dis. 9 (2017) 2344–2349.

[8] H. Pass, D. Giroux, C. Kennedy, et al., The IASLC Mesothelioma Staging Project: improving staging of a rare disease through international participation, J. Thorac. Oncol. 11 (2016) 2082–2088.

[9] A.K. Nowak, K. Chansky, D.C. Rice, et al., The IASLC Mesothelioma Staging Project: proposals for revisions of the T descriptors in the forthcoming eighth edition of the TNM classification for pleural mesothelioma, J. Thorac. Oncol. 11 (2016) 2089–2099.

[10] D. Rice, K. Chansky, A. Nowak, et al., The IASLC Mesothelioma Staging Project: proposals for revisions of the N descriptors in the forthcoming eighth edition of the TNM classification for pleural mesothelioma, J. Thorac. Oncol. 11 (2016) 2100–2111.

[11] V.W. Rusch, K. Chansky, H.L. Kindler, et al., The IASLC Mesothelioma Staging Project: Proposals for the M descriptors and for revision of the TNM stage groupings in the forthcoming (eighth) edition of the TNM classification for mesothelioma, J. Thorac. Oncol. 11 (2016) 2112–2119.

[12] V.W. Rusch, R. Gill, A. Mitchell, D. Naidich, D.C. Rice, H.I. Pass, H.L. Kindler, M. De Perrot, J. Friedberg, Malignant Mesothelioma Volumetric CT Study Group. A multicenter study of volumetric computed tomography for staging malignant pleural mesothelioma, Ann. Thorac. Surg. 102 (2016) 1059–1066.

[13] M.L. Giger, Machine learning in medical imaging, J. Am. Coll. Radiol. 15 (2018) 512–520.

[14] W. Choi, J.H. Oh, S. Riyahi, C.J. Liu, F. Jiang, W. Chen, C. White, A. Rimner, J.G. Mechalakos, J.O. Deasy, W. Lu, Radiomics analysis of pulmonary nodules in low-dose CT for early detection of lung cancer, Med. Phys. 45 (2018) 1537–1549.

[15] Q. Li, J. Kim, Y. Balagurunathan, J. Qi, Y. Liu, K. Latifi, E.G. Moros, M.B. Schabath, Z. Ye, R.J. Gillies, T.J. Dilling, CT imaging features associated with recurrence in non-small cell lung cancer patients after stereotactic body radiotherapy, Radiat. Oncol. 12 (2017) 158.

[16] A. Mansoor, U. Bagci, B. Foster, Z. Xu, G.Z. Papadakis, L.R. Folio, J.K. Udupa, D.J. Mollura, Segmentation and image analysis of abnormal lungs at CT: current approaches, challenges, and future trends, Radiographics 35 (2015) 1056–1076.

[17] M. de Jong, J. Essers, W.M. van Weerden, Imaging preclinical tumour models: improving translational power, Nat. Rev. Cancer 14 (2014) 481–493.

[18] M. de Jong, T. Maina, Of mice and humans: are they the same?–implications in cancer translational research, J. Nucl. Med. 51 (2010) 501–504.

[19] C. Robinson, I. van Bruggen, A. Segal, M. Dunham, A. Sherwood, F. Koentgen, B.W. Robinson, R.A. Lake, A novel SV40 TAg transgenic model of asbestos-induced mesothelioma: malignant transformation is dose dependent, Cancer Res. 66 (2006) 10786–10794.

[20] C. Robinson, A. Walsh, I. Larma, S. O'Halloran, A.K. Nowak, R.A. Lake, MexTAg mice exposed to asbestos develop cancer that faithfully replicates key features of the pathogenesis of human mesothelioma, Eur. J. Cancer 47 (2011) 151–161.

[21] R.J. Francis, T. Segard, L. Morandeau, Y.C. Lee, M.J. Millward, A. Segal, A.K. Nowak, Characterization of hypoxia in malignant pleural mesothelioma with FMISO PET-CT, Lung Cancer 90 (2015) 55–60.

[22] V.W. Rusch, D. Giroux, C. Kennedy, E. Ruffini, A.K. Cangir, D. Rice, et al., Initial analysis of the international association for the study of lung cancer mesothelioma database, J. Thorac. Oncol. 7 (2012) 1631–1639.

[23] N. Corson, W.F. Sensakovic, C. Straus, A. Starkey, S.G. Armato III, Characterization of mesothelioma and tissues present in contrast-enhanced thoracic CT scans, Med. Phys. 38 (2011) 942–947.

[24] H.L. Kindler, N. Ismaila, S.G. Armato 3rd et al., Treatment of malignant pleural mesothelioma: american Society of Clinical Oncology Clinical practice guideline, J. Clin. Oncol. 36 (2018) 1343–1373.

[25] R. Heelan, V. Rusch, C. Begg, et al., Staging of malignant pleural mesothelioma: comparison of CT and MR imaging, AJR Am. J. Roentgenol. 172 (1999) 1039–1047.

[26] T. Frauenfelder, P. Kestenholz, R. Hunziker, et al., Use of computed tomography and positron emission tomography/computed tomography for staging of local extent in patients with malignant pleural mesothelioma, J. Comput. Assist. Tomogr. 39 (2015) 160–165.

[27] H.J. Aerts, E.R. Velazquez, R.T. Leijenaar, et al., Decoding tumour phenotype by noninvasive imaging using a quantitative radiomics approach, Nat Comm 5 (2014) 4006.

[28] M. Bogowicz, O. Riesterer, K. Ikenberg, et al., Computed tomography radiomics predicts hpv status and local tumor control after definitive radiochemotherapy in head and neck squamous cell carcinoma, Int J Radiat Oncol Biol Physics 99 (2017) 921–928.

[29] Z.E. Labby, A.K. Nowak, J.J. Dignam, C. Straus, H.L. Kindler, S.G. Armato III, Disease volumes as a marker for patient response in malignant pleural mesothelioma, Ann. Oncol. 24 (2013) 999–1005.

[30] T. Frauenfelder, M. Tutic, W. Weder, R.P. Götti, R.A. Stahel, B. Seifert, I. Opitz, Volumetry: An alternative to assess therapy response for malignant pleural mesothelioma? Eur. Respir. J. 38 (2011) 162–168.

[31] F. Liu, B. Zhao, L.M. Krug, N.M. Ishill, R.C. Lim, P. Guo, M. Gorski, R. Flores, C.S. Moskowitz, V.W. Rusch, et al., Assessment of therapy responses and prediction of survival in malignant pleural mesothelioma through computer-aided volumetric measurement on computed tomography scans, J. Thorac. Oncol. 5 (2010) 879–884.

[32] O. Ronneberger, P. Fischer, T. Brox, U-Net: convolutional networks for biomedical image segmentation, MICCAI (2015) 234–241.

[33] W.F. Sensakovic, S.G. Armato III, C. Straus, R.Y. Roberts, P. Caligiuri, A. Starkey, H.L. Kindler, Computerized segmentation and measurement of malignant pleural mesothelioma, Med. Phys. 38 (2011) 238–244.

[34] R. Rami-Porta, et al., The IASLC Lung Cancer Staging Project: proposals for the revisions of the T descriptors in the forthcoming eighth edition of the TNM classification for lung cancer, J. Thorac. Oncol. 10 (2015) 990–1003.

[35] H.I. Pass, B.K. Temeck, K. Kranda, S.M. Steinberg, I.R. Feuerstein, Preoperative tumor volume is associated with outcome in malignant pleural mesothelioma, J. Thorac. Cardiovasc. Surg. 115 (1998) 310–317.

[36] R.R. Gill, et al., Epithelial malignant pleural mesothelioma after extrapleural pneumonectomy: stratification of survival with CT-derived tumor volume, AJR Am. J. Roentgenol. 198 (2012) 359–363.

[37] Z.J. Wang, et al., Malignant pleural mesothelioma: evaluation with CT, MR imaging, and PET, Radiographics 24 (2004) 105–119.

[38] M.-A. Weber, et al., Asbestos-related pleural disease: value of dedicated magnetic resonance imaging techniques, Invest. Radiol. 39 (2004) 554–564.

[39] S. Tsim, et al., Diagnostic and Prognostic Biomarkers in the Rational Assessment of Mesothelioma (DIAPHRAGM) study: protocol of a prospective, multicentre, observational study, BMJ Open 6 (2016) e013324.

[40] E. Gudmundsson, C.M. Straus, S.G. Armato III, Deep convolutional neural networks for the automated segmentation of malignant pleural mesothelioma on computed tomography scans, J. Med. Imaging 5 (2018) 034503-1–034503-10.